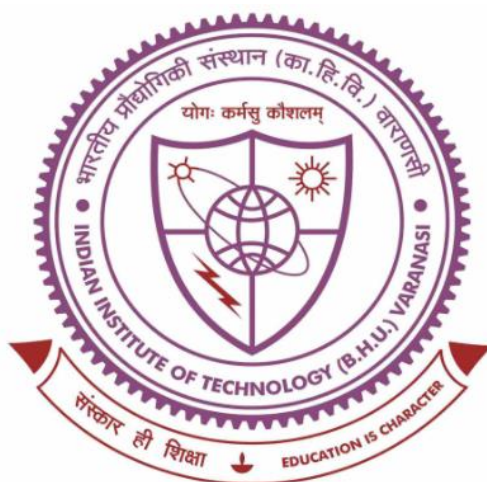


Development of Photo-Ferroelectric Materials for Energy Harvesting and Storage



THESIS SUBMITTED IN PARTIAL FULFILLMENT
FOR THE AWARD OF DEGREE

Doctor of Philosophy

By

Pragyanand Prajapati

School of Materials Science and Technology
Indian Institute of Technology
(Banaras Hindu University)
Varanasi - 221 005

Roll No: 16111008

2022

*Dedicated
To
My Adored Family*

Copyright © Indian Institute of Technology
(Banaras Hindu University), Varanasi, India, 2022.
All rights reserved.



भारतीय
प्रौद्योगिकी
संस्थान
काशी हिन्दू विश्वविद्यालय



INDIAN
INSTITUTE OF
TECHNOLOGY
BANARAS HINDU UNIVERSITY

CERTIFICATE

It is certified that the work contained in the thesis entitles “*Development of Photo-Ferroelectric Materials for Energy Harvesting and Storage*” by “*Pragyanand Prajapati*” has been carried out under my supervision and that this work has not been submitted elsewhere for a degree.

It is further certified that the student have fulfilled all the requirements of comprehensive examination, candidacy and SOTA for the award of Ph.D. degree.

Signature

Supervisor

Dr. Akhilesh Kumar Singh

School of Materials Science and Technology

Indian Institute of Technology

(Banaras Hindu University)

Varanasi -221005

Associate Professor/सह-आचार्य

School of Materials Science & Technology/पदार्थ विज्ञान एवं प्रौद्योगिकी स्कूल

Indian Institute of Technology/भारतीय प्रौद्योगिकी संस्थान

(Banaras Hindu University), Varanasi/काशी हिन्दू विश्वविद्यालय, वाराणसी



भारतीय
प्रौद्योगिकी
संस्थान
काशी हिन्दू विश्वविद्यालय



INDIAN
INSTITUTE OF
TECHNOLOGY
BANARAS HINDU UNIVERSITY

UNDERTAKING FROM THE CANDIDATE

I, **Pragyanand Prajapati**, a research scholar under the supervision of **Dr. Akhilesh Kumar Singh**, Associate Professor, School of Materials Science and Technology, Indian Institute of Technology (Banaras Hindu University), Varanasi, give undertaking that the thesis entitled “**Development of Photo-Ferroelectric Materials for Energy Harvesting and Storage**” submitted by me for the degree of **Doctor of Philosophy** is a record of first-hand research work done by me during the period of study.

I avail myself to responsibility such as an act will be taken on behalf of me, mistakes, errors of facts, and misinterpretations are of course entirely my own.

Date...30/12/2022

Place: Varanasi

Pragyanand
(Pragyanand Prajapati)

DECLARATION BY THE CANDIDATE

I, **Pragyanand Prajapati**, certify that the work embodied in this Ph.D. thesis is my own bonafide work carried out by me under the supervision of **Dr. Akhilesh Kumar Singh** for a period from **July 2016** to **Dec 2022** at the **School of Materials Science and Technology**, Indian Institute of Technology (Banaras Hindu University), Varanasi. The matter embodied in this Ph.D. thesis has not been submitted for the award of any other degree/diploma. I declare that I have faithfully acknowledged and given credits to the research workers wherever their works have been cited in my work in this thesis. I further declare that I have not wilfully copied any other's work, paragraphs, text, data, results, *etc.*, reported in journals, books, magazines, reports dissertations, thesis, *etc.*, or available at websites and have not included them in this thesis and have not cited as my own work.

Date.. 30/12/2022

Place: Varanasi

Pragyanand
(Pragyanand Prajapati)

CERTIFICATE BY THE SUPERVISOR

This is to certify that the above statement made by the candidate is correct to the best of my knowledge.

Ak Singh

(Dr. Akhilesh Kumar Singh)

Supervisor

Associate Professor

School of Materials Science & Technology
IIT (BHU), Varanasi

Associate Professor/सह-आचार्य

School of Materials Science & Technology/पदार्थ विज्ञान एवं प्रौद्योगिकी स्कूल

Indian Institute of Technology/भारतीय प्रौद्योगिकी संस्थान

(Banaras Hindu University), Varanasi/काशी हिन्दू विश्वविद्यालय, वाराणसी

Campy 30/12/22

Coordinator of the School

Coordinator/समन्वयक

School of Materials Science & Technology/पदार्थ विज्ञान एवं प्रौद्योगिकी स्कूल

Indian Institute of Technology/भारतीय प्रौद्योगिकी संस्थान

(Banaras Hindu University), Varanasi/काशी हिन्दू विश्वविद्यालय, वाराणसी

COPYRIGHT TRANSFER CERTIFICATE

Title of the Thesis: “Development of Photo-Ferroelectric Materials for Energy Harvesting and Storage”

Candidate's Name: Pragyanand Prajapati

Copyright Transfer

The undersigned hereby assigns to the Indian Institute of Technology (Banaras Hindu University), Varanasi all rights under copyright that may exist in and for the above thesis submitted for the award of the “ **Doctor of Philosophy**”.

Date: ..30.12.2022
Place: Varanasi

Pragyanand
(Pragyanand Prajapati)

Note: However, the author may reproduce or authorize others to reproduce materials extracted verbatim from the thesis or derivative of the thesis for author's personal use provided that the source and the Institute's copyright notice are indicated.

Acknowledgements

First of all, I would like to express my heartfelt gratitude to my reverent supervisor **Dr. Akhilesh Kumar Singh** for his invaluable guidance, suggestions and motivations during my Ph.D. work. He provided me the freedom for working independently and choosing problems of my interest which made me confident as a researcher. His enthusiasm, patience, encouragement and noble behaviour made me able to continue my research work in the difficult moments of my life.

I would like to pay deep thank to the faculty members of the school, Prof. Dhananjai Pandey, Prof. Rajiv Prakash, Prof. Pralay Maiti, Dr. (Mrs.) Chandana Rath, Dr. Chandan Upadhyay, Dr. Bhol Nath Pal, Dr. Ashish Kumar Mishra, Dr. Shrawan Kumar Mishra, Dr. Sanjay Singh and Dr. Nikhil Singh for their encouragements, suggestions and supports during my Ph.D. work. I would also like to thank Dr. Ashutosh Kumar Dubey, Assistant Professor, Department of Ceramics, Indian Institute of Technology (Banaras Hindu University), Varanasi, India for encouragements, suggestions and supports as an external RPEC member.

I heartily acknowledge to Central Instrumental Facility (CIF), Indian Institute of Technology (Banaras Hindu University), Varanasi, India for providing experimental facilities like - Scanning Electron Microscopy (SEM) along with Energy Dispersive X-ray Spectroscopy, X-ray Photoelectron Spectroscopy etc and their respective operators during my research work.

I would also like to acknowledge my Lab seniors Dr. Rishikesh Pandey, Dr. Ashutosh Upadhyay, Dr. Paramananda Jena, Dr. Sandeep Kumar Singh Patel, Dr. Narendra Kumar Verma, Dr. Umashankar, Dr. Dinesh Kumar, Dr. Chandra bhal Singh, Dr. Sushil Kumar, Dr. Monika Singh for their continuous support and guidance. Among them I would special thank to my senior Dr. Monika Singh for giving me his valuable time to

train me the operation process of machinery and structural analysis using Rietveld refinement. I am also thankful to my friends and colleagues Mr. Manish Kumar, Dr. Shyam Babu, Mr. Ajay Kumar, Mr. Abhishek Tripathi, Mr. Ankit Dwivedi, Dr. Dipti Gangwar, Dr. Mohammad Alam, Mr. Abhay Singh, Dr. Amit Kumar, Mrs. Khushaboo, Ms. Vaishali, and Ms Mamta for their sincere and moral support and suggestions.

In this series I would also like to thank my juniors Mrs. Krishna Prajapati, Ms. Pooja Sonkar, Mr. Vishwa Pratap Singh, Mr. Satyendra Satyarthi, Ms. Srishti Paliwal, Ms. Deep Mala, Mr. Prosun Mondal and Ms. Sadhana Yadav for their ever available cooperation.

I would pay my sincere gratitude to my revered bhैया (Mr. Kailash Prajapati), beloved parents (Mr. Heera Lal Prajapati and Mrs. Anjali Devi) and family members (Mr. Aravind Prajapati, Mrs. Shashikala, Mrs. Sumitra and Mrs. Gayatri) for their patience to bear my long absence from home during my study.

I would like to salute **Mahamana Pandit Madan Mohan Malviya Ji** for establishing this capital of knowledge (BHU). I would fail in my duty if I do not express my gratitude towards all technical and non-technical staff of the School. I express my heartfelt gratitude towards them for all the help they rendered during my stay in the campus. I would also like to thank to all the mess members, who serve my delicious and healthy foods in the last times of my Ph.D. I acknowledge to Department of Science and Technology (DST), India for financial assistance as Junior Research Fellow (JRF) and Senior Research Fellow (SRF) IIT (BHU) is also acknowledged for financial assistance. Finally, I am grateful to **Goddess “Maa Gayatri”** for providing me patience and strength to make this endeavour a success.

. Date:

Sincerely

Place: Varanasi

(Pragyanand Prajapati)

CONTENTS

Chapter 1: Introduction and Literature Survey	1-49
1.1. Motivation and General Introduction	1
1.2 Photovoltaic solar cell	6
1.2.1 Conventional p-n junction photovoltaic cells	6
1.2.2 Ferroelectric Photovoltaic Cells	9
1.2.3 Advantages of Ferroelectric Photovoltaic Cells	12
1.2.4 Limitations of Ferroelectric Photovoltaic effect	12
1.3 Materials used for FEPV solar energy harvesting	13
1.3.1 Perovskite materials	13
1.4. Factors affecting the cell conversion efficiency	16
1.4.1. Mechanism of the energy conversion in solar cell	16
1.4.2 Wavelength of light	16
1.4.3 Band gap	17
1.4.4 Electrical Conductivity	21
1.4.5 Reflection	22
1.4.6 Temperature	22
1.5 Ferroelectricity and its Types	22

1.5.1 Ferroelectricity due to d^0 orbitals	23
1.5.2 Ferroelectricity due to lone pairs	24
1.5.3 Ferroelectricity due to charge ordering	25
1.5.4 Geometrical Ferroelectricity	25
1.5.5 Magnetically Driven Ferroelectrics	26
1.6 Strategies to make efficient ferroelectric photovoltaic materials	27
1.7 An overview of ferroelectric photovoltaic materials	28
1.7.1 Lead Titanate (PbTiO_3) and its solid solutions	30
1.7.2 Bismuth Ferrite (BiFeO_3) based ceramics	33
1.7.2.1 KBiFe_2O_5 Ceramics	36
1.7.2.2 $\text{Bi}_2\text{FeCrO}_6$ Ceramics	38
1.7.3 Barium titanate (BaTiO_3) based ceramics	40
1.7.3.1 Mn-Nb co-doped BaTiO_3	42
1.7.4 Other Attractive Materials	45
1.7.4.1 $(\text{KNbO}_3)_{1-x}(\text{BaNi}_{1/2}\text{Nb}_{1/2}\text{O}_3)_x$ (KNO-BNNO) solid solution	45
1.7.4.2 List of ferro-photovoltaic materials investigated in recent years	46
1.8 BaTiO_3 based ferroelectric materials having energy storage properties	47

1.9 Objective of present work	48
Chapter 2: Experimental Details	50-72
2.1 Introduction	50
2.2. Sample synthesis	50
2.2.1 Solid state reaction method	51
2.2.2 Chemicals used for sample preparation	53
2.3 Characterization Technique	54
2.3.1 X-ray diffraction	54
2.3.1.1 Bragg's Law	56
2.3.1.2 Rietveld Refinement	57
2.3.2 Scanning Electron Microscopy (SEM)	59
2.3.3 Thermal characterization technique (TGA-DTA)	62
2.3.4 X-ray Photoelectron Spectroscopy (XPS)	63
2.3.5 Impedance Spectroscopy	64
2.3.5.1 Permittivity Calculation	65
2.3.5.2 Conductivity estimation from Nyquist plot	66
2.3.6 Ultraviolet-visible (UV-Vis) spectroscopy Characterization	68
2.3.7 Ferroelectric Characterization	70

2.4 Conclusions	71
Chapter 3: Band gap tuning and studies of photo-ferroelectric properties of PbTiO₃ by Mo doping	73-98
3.1. Introduction	73
3.2. Experimental Details	75
3.3. Results and Discussions	76
3.3.1. TGA/DTA Analysis	76
3.3.2. XRD Analysis	78
3.3.3. Microstructural Analysis	83
3.3.4 Band Gap Analysis	85
3.3.5. XPS Analysis	87
3.3.6. Dielectric Analysis	89
3.3.7. DC Conductivity Analysis	92
3.3.8. Ferroelectric Analysis	95
4. Conclusions	98
Chapter 4: Development and characterization of (1-x)BiYO₃-xBiMnO₃ ceramics for Ferro-photovoltaic applications	99-126
4.1. Introduction	99
4.2. Experimental Details	100

4.3. Results and Discussion	101
4.3.1. Thermal Analysis	101
4.3.2. Microstructural Characterization	102
4.3.3. XPS Analysis	106
4.3.4. Crystal Structure Analysis	108
4.3.5. Dielectric Studies	111
4.3.6. Complex Impedance Study	114
4.3.7. Ferroelectric Characterization	119
4.3.8. Band Gap Analysis	123
4.4. Conclusions	125
Chapter 5: Investigation of Bi and Li co-doped $(\text{Bi}_{1/2}\text{Li}_{1/2})_x\text{Ba}_{(1-x)}\text{TiO}_3$ ceramics for energy storage applications.	127-152
5.1. Introduction	127
5.2. Experimental Details	129
5.3. Results and Discussion	131
5.3.1. Crystal Structure Analysis	131
5.3.2. SEM Analysis	134
5.3.3. XPS Analysis	136
5.3.4. Dielectric Analysis	139

5.3.5. Complex Impedance	141
5.3.6. Band Gap Analysis	145
5.3.7. Ferroelectric Characterization	146
5.3.8. Field Dependent Magnetization	154
5.4. Conclusions	151
Chapter 6: Conclusions	153-157
6.1. Summary of the present work	153
6.2. Suggestions for future work	156
References	158-178
List of Publications	179
List of Conferences/Workshops/Seminars/Symposiums	180

List of Figures

Figure No.	Captions	Page No.
Figure 1.1	Global primary energy demand growth by scenario, 2019-2030.	1
Figure 1.2	Intensity variation of solar spectrum.	3
Figure 1.3	Time evolution of efficiencies of several photovoltaic solar cells.	4
Figure 1.4	(a) A typical PN junction diode. (b) Energy level diagram of a PN junction (c) I-V characteristics of the PN junction in the dark and under illumination.	7
Figure 1.5	Schematic diagram showing principle of operation of p-n junction solar cell.	9
Figure 1.6	(a) Schematic diagram showing mechanism in FEPV solar cell (b) I-V characteristic in dark and in light of FEPV solar cell.	10
Figure 1.7	Typical crystal structure of Perovskite.	15
Figure 1.8	Schematic diagram showing the overlapping of orbitals in Si crystal to form the band gap.	18
Figure 1.9	Variation of band gap in BiFeO_3 (ABO_3) perovskite with transition metal doping	18
Figure 1.10	Electronegativity and band gap empirical correlation (X_A and X_B are the electronegativity's of the constituent atoms).	19
Figure 1.11	Energy of d-orbital of transition metal cation (a) in free or isolated ion (b) in field of spherical symmetry (c) with ion in octahedral site (d) with ion in tetrahedral site.	20
Figure 1.12	Off centering of d^0 ion (green circles) and magnetic moment of d^n ions (red arrows) in mixed solid solution.	24
Figure 1.13	Illustration of distortion due to lone pair of Bi.	24
Figure 1.14	Schematic diagram for charge-ordering in ferroelectric materials.	25
Figure 1.15	Schematic diagram for geometrically frustrated distortion.	26

Figure 1.16	(a) The cycloidal spiral spin ordering with the wave vector $Q = Q_x$ and spins rotating in the (x,z)-plane. (b) Co/Mn collinear chain with two states of spin ordering in $\text{Ca}_3\text{CoMnO}_6$.	27
Figure 1.17	Illustration of band gap variation of ferroelectrics materials obtained experimentally with their theoretical polarization.	31
Figure 1.18	(a) Absorption curve and (b) band gap for $\text{PbTi}_{0.95}\text{TM}_{0.05}\text{O}_3$ TM = Mn, Fe and Ni.	31
Figure 1.19	(a) Crystal structure and (b) tetragonality for $\text{PbTi}_{0.95}\text{TM}_{0.05}\text{O}_3$ TM = Mn, Fe and Ni.	32
Figure 1.20	UV-vis diffuse reflectance spectra and the band gap of the sample $\text{Bi}_{1-x}\text{Yb}_x\text{FeO}_3$ with $x = 0.05$.	34
Figure 1.21	(a) Optical absorption of a 100 nm thick BFO film prepared on DyScO_3 substrate at 4 K. (b) Band gap variation as a function of temperature (c) Zoomed view of the shoulder at 2.5 eV.	35
Figure 1.22	UV-Vis-near IR absorption spectrum of KBiFe_2O_5 .	37
Figure 1.23	Variation of maximum theoretical efficiency obtained at a band gap for AM1.5 illumination.	37
Figure 1.24	P-E hysteresis loops of single crystal KBiFe_2O_5 measured at room temperature at increasing applied field ranges.	37
Figure 1.25	Current density curve in the dark and UV illumination.	38
Figure 1.26.	Band gap energy of double perovskite $\text{Bi}_2\text{FeCrO}_6$.	39
Figure 1.27	Comparison of hysteresis Loops of thin film of $\text{Bi}_2\text{FeCrO}_6$ with BiFeO_3 .	39
Figure 1.28	Bulk photovoltaic effect in BaTiO_3 thin film made on MgO substrate (Inset: micro scoping view of the sample).	42
Figure 1.29	J-V characteristics for Pt/ BaTiO_3 /Pt thin film under different illumination.	42
Figure 1.30	(a) Structural evolution of $\text{BaTi}_{1-x}(\text{Mn}_{1/2}\text{Nb}_{1/2})_x\text{O}_3$ series (in red lines) and of $\text{BaTi}_{1-x}(\text{Fe}_{1/2}\text{Nb}_{1/2})_x\text{O}_3$ series (in blue line) (b) Magnified (200) and (002) peak showing tetragonal distortion with Ti substitution.	43
Figure 1.31	Band gap of various compositions of	44

BaTi_{1-x}(Mn_{1/2}Nb_{1/2})_xO₃ compared with Mn replaced by Fe and some other potential photo-ferroelectric materials.

Figure 1.32	Significant room temperature polarization of BaTi _{1-x} (Mn _{1/2} Nb _{1/2}) _x O ₃ with x = 0.50 and 0.75.	44
Figure 1.33	Determination of band gap for KBNNO oxides with x = 0.1–0.5.	45
Figure 1.34	Ferroelectric hysteresis loops for a 20-microm-thick x =0.1 KBNNO film at 77–170 K.	46
Figure 2.1	Flow chart of various steps involved in the solid state synthesis method	52
Figure 2.2	Schematic diagram showing the X-ray diffraction from a crystal lattice plane of a material.	55
Figure 2.3	Image of Scanning electron microscope ZEISS EVO 18.	60
Figure 2.4	Schematic diagram showing the mechanism of SEM.	60
Figure 2.5	Schematic diagram showing the interaction of electron beam to the surface.	61
Figure 2.6	Schematic diagram TGA-DTA analyzer (Mettler Toledo) set up.	62
Figure 2.7	Working principal and experimental set up for XPS spectroscopy.	63
Figure 2.8	Set up of Impedance Analyzer and schematic diagram of an electroded pellet.	65
Figure 2.9	Typical Nyquist plot having semi-circular arcs with intercepts on the real axis giving rise to the corresponding resistances such as Bulk, Grain Boundary and electrode-interface resistances respectively.	68
Figure 2.10	Schematic diagram for set up of UV-Vis spectroscopy	70
Figure 2.11	Hysteresis loop and the Radiant Precision Premier II ferroelectric tester for P-E loop measurement.	71
Figure 2.12	Schematic building block for set up of P-E loop measurement.	71
Figure 3.1	Thermo-gravimetric (TGA) and Differential thermal analysis (DTA) curves of MPT2.5, MPT5, MPT7.5 and	77

MPT10 uncalcined samples.

- Figure 3.2** (a) X-Ray Diffraction Pattern of MPT2.5 and MPT10 samples prepared by low energy and high energy ball milling methods. (b) X-ray diffraction pattern of MPT2.5, MPT5, MPT7.5 and MPT10 calcined at 950°C for 8 hours prepared by HBM method (c) shift in the (101) and (110) XRD peaks in the different synthesis methods 79
- Figure 3.3** Rietveld refinement fits for X-Ray diffraction pattern of MPT2.5, MPT5, MPT7.5 and MPT10. 80
- Figure 3.4** (a) Variation in unit cell parameters ‘a’ and ‘c’ (b) Change in c/a ratio with increasing Mo concentration for MPT samples. 81
- Figure 3.5:** SEM image of the MPT pellets sintered at 1050°C for two hours (a) MPT2.5, (b) MPT5, (c) MPT7.5 and (d) MPT10 and (e) SEM image and EDS spectra of MPT2.5. 84
- Figure 3.6:** (a) $(\alpha h\nu)^2$ versus photon energy (hv) curve for estimation of the band gap (b) Variation of band gap with Mo-doping concentration in PbTiO₃. 86
- Figure 3.7** Core level XPS spectrum of (a) Pb-4f, (b) Ti-2p, (c) Mo-3d and (d) O-1s for MPT10. 89
- Figure 3.8** (a) Temperature-frequency dependence of relative permittivity (ϵ_r) for different compositions MPT2.5, MPT5, MPT7.5 and MPT10. 90
- Figure 3.8** (b) Variation of T_c and tetragonality variation with composition at the same scale. 90
- Figure 3.9** Variation of dielectric loss tangent against temperature-frequency for MPT2.5, MPT5, MPT7.5 and MPT10. 91
- Figure 3.10** (a) Fitted Nyquist plots for MPT2.5, MPT5, MPT7.5 and MPT10 at 45°C. (b) Fitted Nyquist plot for MPT2.5 at different temperatures, the inset shows the magnified part of nyquist plot. 94
- Figure 3.11** (a) Room temperature ferroelectric hysteresis loop of MPT2.5, MPT5, MPT7.5 and MPT10. (b) Room temperature ferroelectric hysteresis loop of MPT5 sample at different frequencies. 97

Figure 4.1	TGA and DTA graphs of uncalcined $\text{BiY}_{(1-x)}\text{Mn}_x\text{O}_3$ ($x = 0.50$) sample.	102
Figure 4.2	SEM micrographs of $\text{BiY}_{(1-x)}\text{Mn}_x\text{O}_3$ pellets sintered at 900°C for two hour (a) $x = 0.0$ (b) $x = 0.10$ (c) $x = 0.25$ (d) $x = 0.75$ and (e) EDX spectrum of $x = 0.75$ sample.	104
Figure 4.2	SEM image of fractured surface of $\text{BiY}_{(1-x)}\text{Mn}_x\text{O}_3$ pellets sintered at 900°C for two hour (f) $x = 0.0$ (g) $x = 0.10$ (h) $x = 0.25$ and (i) $x = 0.75$.	105
Figure 4.3	XPS spectrum of (a) Bi-4f & Y-3d, ($x = 0.25$) (b) Mn-2p ($x = 0.50$) (c) Mn-2p ($x = 0.25$) and (d) O-1s ($x = 0.25$) for $\text{BiY}_{(1-x)}\text{Mn}_x\text{O}_3$ ($x = 0.25$)	108
Figure 4.4	(a) X-ray diffraction pattern of $\text{BiY}_{(1-x)}\text{Mn}_x\text{O}_3$ ($x = 0.0, 0.10, 0.25, 0.50, 0.75$) prepared by high energy ball milling method. Miller Indices are given for the cubic $Fm-3m$ phase. (b) angular shift of the (200) peak with changing Mn concentration.	110
Figure 4.5	(a-d) Refinement fits for X-Ray diffraction pattern of $\text{BiY}_{(1-x)}\text{Mn}_x\text{O}_3$ ($x = 0.0, 0.10, 0.25, 0.50$).	111
Figure 4.6	(a-e) Temperature-frequency dependence of relative permittivity for different compositions of $\text{BiY}_{(1-x)}\text{Mn}_x\text{O}_3$ ($x = 0.0, 0.10, 0.25, 0.50$ and 0.75 , respectively) (f) Loss tangent comparison of samples ($x = 0.10, 0.25, 0.50, 0.75$) near room temperature.	113
Figure 4.7	Fitted Nyquist plots between Z' and Z'' measured at 200°C for $\text{BiY}_{(1-x)}\text{Mn}_x\text{O}_3$ (a) $x = 0.0$ (b) $x = 0.10$ (c) $x = 0.25$ (d) $x = 0.50$ and (e) $x = 0.75$.	117
Figure 4.7	Fitted Nyquist plots at different temperatures for $\text{BiY}_{(1-x)}\text{Mn}_x\text{O}_3$ (f) $x = 0.10$, (g) $x = 0.75$ and (h) Arrhenius plot of dc conductivity for $x = 0.10, 0.50$ and $x = 0.75$.	118
Figure 4.8	Room temperature P-E loops measured at different field strength at 200Hz for $\text{BiY}_{(1-x)}\text{Mn}_x\text{O}_3$ (a) $x = 0.0$ (b) $x = 0.10$ (c) $x = 0.25$ (d) $x = 0.50$ (e) $x = 0.75$ and (f) combined P-E loops of $\text{BiY}_{(1-x)}\text{Mn}_x\text{O}_3$ ($x = 0.0, 0.10, 0.25, 0.50$) compositions measured at 200Hz and 40 kV/cm .	122

Figure 4.9	Fig. 4.9. (a) Optical absorption curves, (b) Tauc plots with extrapolated band gap and (c) Composition dependence of band gap for $\text{BiY}_{(1-x)}\text{Mn}_x\text{O}_3$ ceramics.	125
Figure 5.1	X-ray diffraction pattern of calcined sample $(\text{Bi}_{0.5}\text{Li}_{0.5})_x\text{Ba}_{(1-x)}\text{TiO}_3$ ($x = 0.10, 0.12, 0.15, 0.20$ and 0.25).	131
Figure 5.2	Rietveld refinement fits for X-Ray diffraction pattern of $(\text{Bi}_{0.5}\text{Li}_{0.5})_x\text{Ba}_{(1-x)}\text{TiO}_3$. (a) $x = 0.10$, (b) $x = 0.12$, (c) $x = 0.15$, (d) $x = 0.20$ and (e) $x = 0.25$ (f) Variation of Lattice parameter and volume with different composition.	132
Figure 5.3	(a-d) SEM micrographs of $(\text{Bi}_{0.5}\text{Li}_{0.5})_x\text{Ba}_{(1-x)}\text{TiO}_3$ ($x = 0.10, 0.12, 0.15$ and 0.20) pellets sintered at 950°C	135
Figure 5.3	(e-h) particle distribution of $(\text{Bi}_{0.5}\text{Li}_{0.5})_x\text{Ba}_{(1-x)}\text{TiO}_3$ ($x = 0.10, 0.12, 0.15$ and 0.20) pellets sintered at 950°C .	136
Figure 5.4:	XPS spectrum of (a) Bi-4f (b) Li-1s (c) Ba-3d (d) Ti-2p (e) O-1s and (f) Full scan elemental survey for $(\text{Bi}_{0.5}\text{Li}_{0.5})_x\text{Ba}_{(1-x)}\text{TiO}_3$ ($x = 0.12$).	138
Figure 5.5	(a-e) Relative permittivity variation with temperature at various frequency for different compositions of $(\text{Bi}_{0.5}\text{Li}_{0.5})_x\text{Ba}_{(1-x)}\text{TiO}_3$ ($x = 0.10, 0.12, 0.15, 0.20$ and 0.25)	140
Figure 5.5	(f) Frequency variation of dielectric constant at 100°C (g) Temperature variation of permittivity for different compositions at 10^3 Hz of $(\text{Bi}_{0.5}\text{Li}_{0.5})_x\text{Ba}_{(1-x)}\text{TiO}_3$ ($x = 0.10, 0.12, 0.15, 0.20$ and 0.25).	141
Figure 5.6	Fitted Nyquist plots for $(\text{Bi}_{0.5}\text{Li}_{0.5})_x\text{Ba}_{(1-x)}\text{TiO}_3$ ($x = 0.10, 0.12, 0.15, 0.20$ and 0.25) measured at 500°C (a) $x = 0.10$ (b) $x = 0.12$ (c) $x = 0.15$ (d) $x = 0.20$ and (e) $x = 0.25$.	142
Figure 5.6	(g-j) Fitted Nyquist plots at different temperatures 400°C , 300°C , 200°C , 100°C and 50°C for $(\text{Bi}_{0.5}\text{Li}_{0.5})_x\text{Ba}_{(1-x)}\text{TiO}_3$ $x = 0.20$.	143
Figure 5.7	Tauc plots with extrapolated band gap for $(\text{Bi}_{0.5}\text{Li}_{0.5})_x\text{Ba}_{(1-x)}\text{TiO}_3$ ($x = 0.10, 0.12, 0.15, 0.20$ and 0.25) ceramics	146
Figure 5.8	Room temperature P-E loops measured at 10Hz for $(\text{Bi}_{0.5}\text{Li}_{0.5})_x\text{Ba}_{(1-x)}\text{TiO}_3$ (a) $x = 0.10$ (b) $x = 0.12$ (c) $x = 0.15$ (d) $x = 0.20$ (e) $x = 0.25$ (f) combined P-E loops of	147

$(\text{Bi}_{0.5}\text{Li}_{0.5})_x\text{Ba}_{(1-x)}\text{TiO}_3$ ($x = 0.10, 0.12, 0.15, 0.20$ and 0.25)
compositions recorded at 10Hz .

- Figure 5.8** Room temperature P-E loops measured at different frequency for $(\text{Bi}_{0.5}\text{Li}_{0.5})_x\text{Ba}_{(1-x)}\text{TiO}_3$ (g) $x = 0.15$ and (h) $x = 0.25$ 148
- Figure 5.9** P-E hysteresis loop showing the stored energy density and energy loss density for P-E loop of $(\text{Bi}_{1/2}\text{Li}_{1/2})_{0.12}\text{Ba}_{0.88}\text{TiO}_3$ ceramics at (a) 80kV and (b) 70kV. 150

List of Tables

Table No.	Captions	Page No.
Table 1.1	Structure and piezoelectric physical properties of Bi site doped BiFeO ₃ ceramics.	34
Table 1.2	Structure and piezoelectric physical properties of Fe site doped BiFeO ₃ ceramics.	34
Table 1.3	Performance of single layer Bi ₂ FeCrO ₆ devices.	40
Table 1.4	List of the experimental band gap of various pure and doped ferroelectric materials.	47
Table 2.1	List of the raw materials used for preparation of different samples.	53
Table 3.1	Structural parameters and agreement factors obtained after Rietveld structure refinement for MPT2.5, MPT5, MPT7.5 and MPT10.	82
Table 3.2	Displacement of ions in various compositions of MPT.	82
Table 3.3	DC impedance and DC conductivity of MPT2.5, MPT5, MPT7.5 and MPT10 at 45°C.	95
Table 3.4	DC impedance and DC conductivity of MPT2.5 at various temperatures.	95
Table 4.1	Refined structural parameters for BiY _(1-x) Mn _x O ₃ (x = 0.0, 0.10,0.25,0.50).	111
Table 4.2	DC impedance and DC conductivity of BiY _(1-x) Mn _x O ₃ for different compositions.	118
Table 4.3	DC impedance and DC conductivity of BiY _(1-x) Mn _x O ₃ (x = 0.10, x = 0.75) at various temperatures	119
Table 5.1	List of refinement parameters and unit cell parameters obtained after Rietveld structure refinement for (Bi _{0.5} Li _{0.5}) _x Ba _(1-x) TiO ₃ .	133
Table 5.2	DC impedance and conductivity of (Bi _{0.5} Li _{0.5}) _x Ba _(1-x) TiO ₃ (x = 0.10, 0.12, 0.15 , 0.20 and 0.25)	144
Table 5.3	DC impedance and DC conductivity of (Bi _{0.5} Li _{0.5}) _x Ba _(1-x) TiO ₃ (x = 0.20) at various temperatures	144
Table 5.4	Comparison of energy storage density and energy storage	149

efficiency for different compositions at applied field 60
kV/cm

Table 5.5 Comparison of W_C and η from earlier reports in literature 150

List of Symbols and Abbreviations

α	Absorption Coefficient
IR	Infrared
λ	Wavelength
Vis	Visible
UV	Ultraviolet
T_c	Curie Temperature
EDS	Energy dispersive X-ray spectroscopy
XRD	X-ray Diffraction
SEM	Scanning Electron Microscope
J-T	Jahn-Teller
P_s	Saturated Polarization
P_r	Remanant Polarization
E_c	Coercive Electric Field
J_{sc}	Short circuit Current density
V_{oc}	Open Circuit Voltage
ME	Magneto-Electric
FF	Fill factor
TM	Transition Metal
PV	Photo-voltaic

Preface

Solar energy is a most abundant, free, clean and sustainable energy source which can be directly utilized through the photovoltaic (PV) effect. If technological advancement can utilize only 0.2% of the solar radiation falling on earth every second with 10% efficiency, it will produce 24 terawatts, sufficient to fulfil the societal needs. However, limitation of efficiency in conventional Si-based photovoltaic solar cells, toxic waste and CO₂ emission during photovoltaic panel production limit their contribution in the current energy supply market. Emerging photovoltaic technologies such as ferroelectric perovskite solar cells have drawn great attention for their low-cost manufacturing techniques and for possibility of brisk increases of power conversion efficiency up to 25%. Efficiency of conventional PV technologies mainly depends upon the barrier field strength at the p-n junctions which separates the charge carriers, and band gap of the semiconductor. Maximum efficiency of conventional PV technologies that can be achieved is limited by Shockley-Queisser limit. The charge separating electric field i.e., the barrier electric field is formed at the time of manufacture of the p-n junction and cannot be controlled externally. However, a different PV mechanism in ferroelectric photovoltaic materials is present; here photovoltage is not constrained to inbuilt internal barrier fields. In ferroelectric materials, separation of photo-excited charge carriers is done by polarization induced electric field and this field is present throughout the entire crystal and hence also known as the ‘‘bulk photovoltaic effect’’ (BPVE). This property of ferroelectric based solar cells can create above-band gap open-circuit voltages which is not possible in the conventional solar cells. In spite of these attractive properties, there are many challenges in ferroelectric photovoltaic materials like high band gap, low conductivity, device fabrication etc. which restricts their efficiency to remain lower than the conventional solar cells. These challenges demand more research and investigation

on ferroelectric photovoltaic materials. A key challenge is to reduce the wide band gap of ferroelectric material to make suitable for exploring visible range spectrum without compromising the ferroelectric properties. Thus a proper designing of ferroelectric material is required via band gap engineering. The band gap engineering in these systems could potentially be approached through chemical substitution, cation ordering, quantum size effects, lattice mismatch or super lattice formation.

To achieve these goals outlined above, we focused our investigation on the **“Development of Photo-Ferroelectric Materials for Energy Harvesting and Storage”** for this Ph.D. thesis. Our motive is to modify the properties of typical ferroelectrics like PbTiO_3 , BaTiO_3 and Bi-based perovskite materials in such a way that they become useful for ferro-photovoltaic applications. Our detailed investigations on various materials have led to several new findings in the field of ferro-photovoltaic oxide materials. A brief summary of important findings from our investigation on various developed systems in this thesis work is discussed below:

In **Chapter 1**, the requisite fundamental concepts, knowledge and literature survey are discussed in a detailed and systematic way. This chapter starts with illustrating how the energy demand of the world is increasing year by year and still the major source to fulfil this demand is fossil fuels. Then the contribution of renewable energy sources especially the contribution of solar cells is described here. Different types of solar cells along with their efficiencies are compared together and main focus has been paid to ferroelectric photovoltaic solar cells which have great potential to increase the efficiency. The working principle and the advantages of ferroelectric photovoltaic solar cells over conventional solar cells is discussed in detail. Then the physical properties that an ideal photo-ferroelectric material should possess are described. Further, the different type of ferroelectricity and ferroelectric materials are narrated in detail. A brief

review on Pb-based and Pb-free photo-ferroelectric materials has also been carried out in this chapter. In this sequence, we have discussed many interesting photo-ferroelectric materials, which have low band gap and good conversion efficiency. Finally, we have outlined the objective of our research work on ferroelectric photovoltaic oxide materials.

In **Chapter 2**, we have discussed the experimental method of sample preparation and different techniques used to characterize the sample along with their working principle. The TGA-DTA measurement, Scanning electron microscopy, X-ray diffraction measurement and X-ray photoemission spectroscopy have been employed for thermal, morphological, structural, phase, elemental and chemical state analysis. UV-vis spectroscopy and Tauc plots using Kubelka Munk function for the band gap determination has been described. Temperature dependent permittivity and ac resistance were determined from the frequency and temperature dependent complex impedance measurement. At the end of this chapter, polarization (P)-Electric field (E) hysteresis loop measurements are discussed which is performed to see the ferroelectric nature and polarization properties of the sample.

In **Chapter 3**, the results of investigation on PbTiO_3 based material is described in detail. Crystal structure, micro-structural, optical, dielectric and ferroelectric properties have been investigated on various compositions of $\text{PbTi}_{1-x}\text{Mo}_x\text{O}_3$ ($x = 0.025, 0.050, 0.075, 0.100$). All Mo-doped PbTiO_3 powder samples were synthesized by solid state method using high energy ball milling process. Structural analysis shows all samples crystallize into tetragonal phase and unit cell parameters change in such a way that c/a ratio increases with increasing substitution concentration. The microstructure of the sintered samples exhibit agglomerated grains leading to non-uniformity in grain size distribution. Temperature dependent permittivity curve reveals that Curie temperature

(T_c) slightly increases with increasing Mo-substitution concentration which is in consistence with the increase in tetragonality i.e., c/a ratio as revealed by XRD analysis. UV-Vis spectroscopy shows that Mo-substitution in $PbTiO_3$ reduces the band gap significantly without influencing the ferroelectric properties. The P-E hysteresis loops of all the samples show the ferroelectric nature of the material and increasing tetragonal distortion (c/a ratio) with Mo-incorporation implies increase in polarization. So enhanced polarization in Mo-substituted samples will result in more efficient separation of charge carriers. Mo-substitution in $PbTiO_3$ also increases the conductivity which will help the charge carriers, separated by polarization field to reach their respective electrodes.

In **Chapter 4**, we have tried to design a Bi-based novel material compositions $BiY_{(1-x)}Mn_xO_3$ ($x = 0.0, 0.10, 0.25, 0.50, 0.75$) that have low band gap, good conductivity and significant ferroelectric polarization. The samples were synthesized by solid state method using ball milling process. Structural, morphological, optical, dielectric, electrical and ferroelectric properties of $BiY_{(1-x)}Mn_xO_3$ were analyzed using different characterization techniques. XRD analysis shows that most of the samples (except $x = 0.75$), were indexed with cubic fluorite structure and $Fm3m$ space group. Here, we observed that one of the composition $x = 0.50$ has sufficiently low band gap (1.76 eV) and significant ferroelectric polarization. Conductivity of the samples were also found to increase with increase in Mn- concentration as well as with increasing temperature showing semiconducting behavior of the developed system.

In **Chapter 5**, we have discussed structural, morphological, dielectric, transport, impedance and ferroelectric properties of polycrystalline lead free material $Ba_{(1-x)}(Bi_{0.5}Li_{0.5})_xTiO_3$ ($x = 0.10, 0.12, 0.15, 0.20, 0.25$). The material crystallizes into pseudocubic perovskite structure with space group $Pm-3m$. Microstructural analysis of

the samples suggests a spheroid shaped non-porous grains with homogeneous grain size distribution. Temperature dependent permittivity curve of all the compositions reveal absence of any high temperature phase transition. This is consistent with XRD analysis results showing the most symmetric cubic crystal structure for all the compositions at room temperature. One of the composition ($x = 0.12$) is found to have exceptionally high permittivity among all doped compositions. Nyquist plot for all the compositions show a single semicircular curve, the radius of which increases with increasing Bi-Li concentration and decreases with rise in temperature confirming semiconducting behavior. The band gap decreases at first and then starts increasing with increasing Bi-Li co-substituent concentration. Ferroelectric analysis of various compositions showed slim and slanted P-E loops with significant polarization, suitable for energy storage applications. The two compositions of $\text{Ba}_{(1-x)}(\text{Bi}_{0.5}\text{Li}_{0.5})_x\text{TiO}_3$ with $x = 0.12$ and 0.25 have shown extraordinary storage efficiency of $\sim 95\%$ and 96% with good energy storage density which seems to be promising material for energy storage devices.

In **Chapter 6**, a brief summary of the important findings of the present thesis and possibility of future work in this research field, have been discussed.

